# Compare three different algorithms (MOPSO, SPEA2, NSGA-II) for Multi Objective Optimization of a novel Combined Cooling, Heating, and Power (CCHP) system based on organic Rankine cycle

**Reza Asadi[1], Ehsanolah Assaerh[1,2*], Reza Poultangari[1,2] , Ali Heidary Moghadam[2], Rahim Moltames[3],**

**Tahereh pirhoushyaran[4]**

[1]Department of Mechanical Engineering, Dezful Branch, Islamic Azad University, Dezful, Iran

[2]Materials and Energy Research Center, Dezful Branch, Islamic Azad University, Dezful, Iran

[3]Department of Energy Engineering, Energy Systems Engineering, Sharif University of Technology, Tehran, Iran

[4]Department of Chemical Engineering, Dezful Branch,Islamic Azad University,Dezful,Iran

## Abstract

Recently Debates about Energy and the issue of global warming have led to the use of new energy. One of the best options for this purpose is the use of a new hybrid system of power, heating and refrigeration, with its thermal source of solar and geothermal energy. In the present study, used a combined cooling, heating and power system based on the organic Rankine cycle and the Ejector Refrigeration subsystem, which utilizes solar energy to supply energy and for pre-heating used the geothermal energy, proposed for supply cooling energy, heat energy and electrical power for the building in the south of the Iran (Behbahan city). In this proposed system, used the copper oxide/water nano-fluids in the flat plate solar collector, and used the R245fa, R123, R134a, and R600a in the CCHP system have been investigated as operating fluid. By analyzing the thermodynamic and thermos-economic sensitivity of the whole system, the effect of the volume fraction of the nanoparticle volume concentration CuO, the turbine inlet pressure, the solar collector surface, the solar collector tilt angle and the temperature difference of the steam generator pinch point checked for the four desired target functions (daily heat efficiency, Daily exergy efficiency, total heat exchanger surface, and total cost of the product). we found that the R123 fluid is the best refrigerant from the perspective of energy and exergy (maximum thermal and exergy efficiency) and the R600a refrigerant has the lowest level of heat exchangers and the best fluid from the economic point of view (minimum cost of total products).

**Key words:** solar energy, nano-fluid, optimization, CCHP system

*corresponding author: assareh@iaud.ac.ir

## 1- Introduction

In recent years, the number of studies carried out on the different types of CCHP systems has increased due to the relevance of these systems in saving energy resources and reducing the environmental pollution. CCHP systems have higher productivity, less environmental pollution and improved security against unpredictable events, such as earthquakes, wars and so on, compared to separate systems for generation of cold, heat and power. El-Emam et al, conducted an economic and thermodynamic analysis on a geothermal system in Turkey and designed a converter for organic fluids using the concepts of energy and exergy. Energy values and exergy efficiency calculated at the optimum state were 37.16% and 8.48%, and the mass rates of organic fluid [1]. Haeseldonckx et al. [15] showed that using a storage tank prolongs the annual operation time in CHP installations and allows for constant activity of the PGU. They showed that TES reduces $CO_2$ emission by 1/3 of the reference sample without heat buffer. Wang and Ma [16] stated that a proper design for optimization systems should include a thermal energy saver. Modified linear programming has been widely used in previous studies for TES. Although, non-linear or dynamic programming can also be used, they need longer time to solve the problem or force convergence due to the large number of variables [17]. Henze et al. [18] developed an optimization strategy for water cooling units by a heat saver and used dynamic programming for optimization of cooling load to optimize the strategy of charge / discharge of the TES system. Yongliang et al. [19] studied a thermal energy storage system that saves surplus energy of the triple system in the form of compressed air and heating. They reported that the proposed system is very promising for practical applications, especially for renewable resources, due to its simple configuration and flexibility. Kian and Sedaghat [20] stated that a hybrid GCHP can be used as a solution to eliminate the problems associated with sizing conventional GCHP systems when heating and cooling loads are very high. Park et al. [21] analyzed the optimization of a combined hybrid GCHP with a cooling tower and concluded that performance coefficient and heat dissipation ratio in hybrid systems are 21% and 42% higher and lower, respectively, than those of a conventional GCH. Alavi et al. [22] suggested a method for optimizing hybrid heat pumps and used it in10 different projects in order to reduce initial costs, capital return and operating costs and concluded that the proposed method can supply 80% of total capital cost.Li et al, conducted a thermo-economic analysis and compared a $CO_2$ power cycle and an organic Rankine cycle. They

concluded that the ground heat resource at low temperature for the organic fluid has an acceptable power [2]. Reyes et al, examined theoretically and experimentally the exergy of the solar heat pump system for heating air. They proposed a method for optimizing the evaporation and condensation temperatures of the refrigerant R22 [3]. Badescu [4] used the second law of thermodynamics to investigate the exergy of the direct expansion solar heat pump water heater and calculated system exergy efficiency values and exergy loss factors for each component. Dikici and Akbulut [5] conducted theoretical and experimental studies on a solar heat pump system at ambient conditions in Elazig city, Turkey. They reported second law efficiencies for compressor, condenser, evaporator and solar collector, i.e., 1.42%, 7.83%, 2.43% and 4.9%, respectively, and assessed the entire system exergy efficiency as 8.30%. The results show that thermal performance coefficient of the system increases as the amount of exergy losses in the evaporator are reduced.

## 2- System description

The proposed system, as shown in Fig. 1, consists of two main subsystems including a solar collector subsystem and a combined power, heating, and ejector refrigeration subsystem (CCHP subsystem). The CCHP subsystem consists of eight components: generator, turbine, heater, pumps, condenser, ejector, evaporator and expansion valves. The working fluid is pumped as the saturated liquid to the vapor generator (point 1) and its pressure is increased to the working pressure of the vapor generator (point 2). The high pressure and high temperature of the vapor generator are provided by heat generated from thermal resources including solar energy and geothermal energy. The output vapor of the vapor generator is expanded in the turbine and generates the mechanical output power of the entire system (point 3). The fluid in the turbine outlet (point 4) enters the heater heat exchanger to supply the heat for heating purposes. In order to provide demand cooling, the output condensed vapor of the condenser is separated into two flows. One flow returns back to the pump and the other flow goes to the expansion valve (point 8) and its pressure and temperature are decreased to the working pressure and temperature of the evaporator (point 9). Then the working fluid enters the evaporator to refrigeration by absorbing heat from the cold water.The solar collector subsystem includes a flat plate collector, a storage tank, and auxiliary boiler. Flat plate solar collectors are very common in domestic applications for its high performance and low cost. The storage tank is used to save energy in the case that the energy produced by the solar collectors are greater than the energy demand

of the entire system in order that the system can supply energy sustainably. The solar collector subsystem uses water/ copper-oxide nanofluid as the working fluid. Nanofluids, which are derived from the distribution of nanoparticles in conventional fluids, are a new generation of highly efficient fluids in industrial applications. The particles size used in nanofluids are from 1 nm to 100 nm. These nanoparticles include metal particles such as copper (*Cu*), silver, etc., or metal oxides such as aluminum oxide (*Al₂O₃*), copper oxide (*CuO*), and so on. Conventional heat transfer fluids commonly have a low thermal conductivity coefficient. Nanoparticles, due to their high conductivity and distribution in the base fluid (conventional fluids like water), increase the thermal conductivity of the fluid, which is considered as the fundamental parameter of heat transfer. Results of experimental researches show that adding nanoparticles to base fluid significantly increases the heat transfer coefficient in a nanofluid. Therefore, nanotubes are suitable alternatives for use in heat transfer applications. On the other hand, these nanoparticles have more stable suspensions than particles in micrometric dimensions. The heat transfer analysis was carried out using a nanofluid with a volumetric concentration of nanoparticles (φ) between 0 and 2% (water is considered as the base fluid). see Ref. [6] for analyzing the equations of heat transfer of nanoparticles. The values of the input parameters used in the simulation of the proposed system are shown in Table 1.
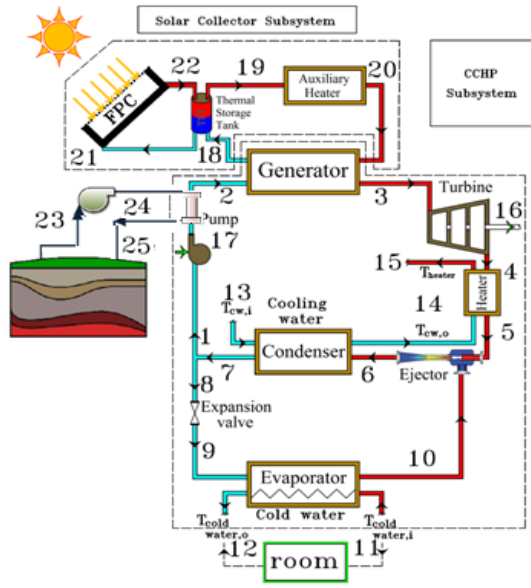


**Figure 1.** The detailed layout of the proposed combined system [7].

## 3- System performance

The performance of the combined system can be analyzed using thermal and exergy efficiency. The real thermal efficiency of the system is defined as the ratio of the useful output energy to the total input energy of the system, given by:

$$\eta_{ins\,tant} = \frac{\dot{W}_{out}}{\dot{E}_{in}} = \frac{\dot{W}_{NET} + \dot{Q}_e + \dot{Q}_{heater} + \dot{Q}_{con}}{\dot{E}_{in}} \qquad (1)$$

The daily thermal efficiency is a better index than real thermal efficiency to evaluate the performance of the system and is given by the following equation:

**Table 1. Input data for the system**

| Description | Parameter | Value |
|---|---|---|
| Ambient temperature | $T_a(K)$ | 296.98 |
| Ambient pressure | $P_a(kPa)$ | 101.325 |
| Solar radiation | $H(J/m^2.h)$ | 28242 |
| Clearness index | $K_T$ | 0.677 |
| Pump isentropic efficiency | $\eta_P(\%)$ | 85 |
| Turbine isentropic efficiency | $\eta_T(\%)$ | 8 |
| Pinch point temperature difference | $\Delta T_{Pinch}(°C)$ | 6.6 |
| The ejector nozzle efficiency | $\eta_n(\%)$ | 85 |
| The ejector mixing efficiency | $\eta_m(\%)$ | 75 |
| The ejector diffuser efficiency | $\eta_d(\%)$ | 85 |
| Turbine inlet pressure (R600a) | $P_3(kPa)$ | 1500 |
| Turbine inlet pressure (R245faa) | $P_3(kPa)$ | 1500 |
| Turbine inlet pressure (R123) | $P_3(kPa)$ | 700 |
| Turbine inlet pressure (R134a) | $P_3(kPa)$ | 2100 |
| The outer diameter of collector pipes | $D_{O,FPC}(m)$ | 0.018 |
| The internal diameter of collector pipes | $D_{i,FPC}(m)$ | 0.014 |
| The distance between collector pipes | $W_{FPC}(m)$ | 0.08 |
| Solar collector dimensions | $L_1*L_2(m^2)$ | 2.99 (2.444*1.223) |
| Number of solar collectors | $N_{FPC}$ | 132 |
| Flat plate solar collector area | $A_{FPC}(m^2)$ | 395 |
| Storage tank outer diameter | $D_{O,TST}(m)$ | 2.1 |
| Storage tank internal diameter | $D_{i,TST}(m)$ | 1.7 |
| The storage tank wall thickness | $t_{TST}(m)$ | 0.006 |
| The tilt angle of solar collectors | $\beta(°)$ | 13 |
| Hydraulic diameter | $D_h=2b(m)$ | 0.008 |

| | | |
|---|---|---|
| Plate heat exchanger width | W(m) | 1 |
| Plate heat exchanger thickness | $d_p$(m) | 0.002 |
| The thermal conductivity of heat exchangers | $k_{plate}$-$k_{tube}$(W/mK) | 14.9-401 |
| Shell and tube heat exchanger outer diameter | $D_{O,tube}$(m) | 0.015 |
| Shell and tube heat exchanger internal diameter | $D_{i,tube}$(m) | 0.013 |

$$\eta_{th} = \frac{\int \dot{W}_{out}(t)dt}{\int \dot{E}_{in}(t)dt} \tag{2}$$

The time interval of the integral in the above equation is a day. In thermodynamics, exergy is the maximum possible amount of work that a system can produce and the exergy efficiency is defined as the ratio of the output exergy to the input exergy of the entire cycle which is calculated by the following equation:

$$\eta_{ex} = \frac{\int (\dot{W}_{NET} + \dot{Ex}_e + \dot{Ex}_{heater} + \dot{Ex}_{con})dt}{\int \dot{Ex}_{in}dt} \tag{3}$$

$\dot{Ex}_{in}$ in the above equation is the sun exergy and is calculated by the following equation [8], [9]:

$$\dot{Ex}_{in} = A_{Sc}G_t(1 + \frac{1}{3}(\frac{T_0}{T_{Sun}})^4 - \frac{4}{3}(\frac{T_0}{T_{Sun}})) \tag{4}$$

Where sun temperature ($T_{sun}$) is 6000K.

## 4- Thermoeconomic analysis

In economic analysis, the cost balance for each component of the system is written as follows:

$$\sum_{out} \dot{C}_{out,k} + \dot{C}_{w,k} = \dot{C}_{q,k} + \sum_{in} \dot{C}_{in,k} + \dot{Z}_k \tag{5}$$

$$\dot{C}_i = c_i \dot{E}_i \tag{6}$$

$$\dot{Z}_k = \dot{Z}_k^{CI} + \dot{Z}_k^{OM} \tag{7}$$

The cost balance (Eq. 5) shows that the total cost of output exergies is equal to the total cost of input exergies plus the investment and maintenance costs. All terms of the Eq. 5 are positive. Cost balance equations for each component of the system are shown in Table 2. The investment cost of the system in the present study includes the cost of purchasing components, installation costs, insulating costs, plumbing costs, and the cost of the control system. For each component of the system, it is expected to increase its investment cost by increasing its capacity or efficiency. The investment costs of combined system components are given by the following equations:

**Pump** [10]:

$$Z_P(\$) = 3540\,\dot{W}_P^{0.71} \tag{8}$$

**Heater, evaporator, and vapor generator** [10]:

$$Z_{HE}(\$) = 130\left(\frac{A_{HE}}{0.093}\right)^{0.78} \tag{9}$$

**Condenser:**

$$Z_c(\$) = 1773\,\dot{m}_{r,c} \tag{10}$$

**Turbine** [11]:

$$Log_{10}(Z_T)(\$) = 2.6259 + 1.4398\log_{10}(\dot{W}_T) - 0.1776[Log_{10}(\dot{W}_T)]^2 \tag{11}$$

**Table 2. Cost balance and auxiliary equations for each component of the system**

| Component | Cost balance equation | Auxiliary equation |
|---|---|---|
| Pump | $\dot{C}_2 - \dot{C}_1 - \dot{C}_{W_P} = \dot{Z}_P$ | $\dfrac{\dot{C}_{W_P}}{\dot{W}_P} = \dfrac{\dot{C}_{W_T}}{\dot{W}_T}$ |
| Vapor generator | $\dot{C}_3 - \dot{C}_2 - \dot{C}_{19} + \dot{C}_{18} = \dot{Z}_g$ | $\dfrac{\dot{C}_{19}}{\dot{E}_{19}} = \dfrac{\dot{C}_{18}}{\dot{E}_{18}}$ |
| Turbine | $\dot{C}_{W_T} - \dot{C}_3 + \dot{C}_4 = \dot{Z}_T$ | $\dfrac{\dot{C}_3}{\dot{E}_3} = \dfrac{\dot{C}_4}{\dot{E}_4}$ |
| Heater | $\dot{C}_{15} - \dot{C}_{14} - \dot{C}_4 + \dot{C}_5 = \dot{Z}_h$ | $\dfrac{\dot{C}_4}{\dot{E}_4} = \dfrac{\dot{C}_5}{\dot{E}_5}$ |
| Ejector | $\dot{C}_6 - \dot{C}_5 - \dot{C}_{10} = \dot{Z}_{ejc}$ | - |
| Condenser | $\dot{C}_{14} - \dot{C}_{13} - \dot{C}_6 + \dot{C}_7 = \dot{Z}_c$ | $\dfrac{\dot{C}_6}{\dot{E}_6} = \dfrac{\dot{C}_7}{\dot{E}_7}$ |
| Expansion valve and evaporator | $\dot{C}_{12} - \dot{C}_{11} - \dot{C}_8 + \dot{C}_{10} = \dot{Z}_e + \dot{Z}_{exv}$ | $\dfrac{\dot{C}_8}{\dot{E}_8} = \dfrac{\dot{C}_9}{\dot{E}_9}$ $\dfrac{\dot{C}_8}{\dot{E}_8} = \dfrac{\dot{C}_{10}}{\dot{E}_{10}}$ |
| Thermal storage tank | $(\dot{C}_{21} + \dot{C}_{19}) - (\dot{C}_{22} + \dot{C}_{18}) + \dot{C}_{L,ST} = \dot{Z}_{ST}$ | $\dfrac{\dot{C}_{19}}{\dot{E}_{19}} = \dfrac{\dot{C}_{21}}{\dot{E}_{21}}$ |
| Solar collector | $\dot{C}_{22} - \dot{C}_{21} - \dot{C}_{F,Sc} = \dot{Z}_{Sc}$ | $\dot{C}_{F,Sc} = 0$ |

**Flat plate solar collector[2]:**

$$Z_{FPC}(\$) = 550 \, N_{Sc} \qquad (12)$$

**Thermal storage tank [12]:**

$$Z_{ST}(\$) = 4042 \, .Vol_{ST}^{0.506} \qquad (13)$$

In thermoeconomic analysis, all costs must be updated to the specified year as the base year. The cost index is used to update the cost values given by the following equation [14]:

$$C_B = C_O \times \frac{CI_B}{CI_O} \qquad (14)$$

In this study, the cost indices provided by Marshall and Swift in 2013 are used to update costs [13].

The cost rate for the kth component of the system is calculated as follows:

$$\dot{Z}_k = \left( \frac{Z_k.CRF.\phi}{t * 3600} \right) \qquad (15)$$

Where $\varphi$ is the maintenance factor (=1.06), and t is the number of operating hours of the system in a year (=7446 hours).

$CRF$ in Eq. (15) is the capital recovery factor and is given by:

$$CRF = \frac{i(1+i)^N}{(1+i)^N - 1} \qquad (16)$$

The system lifetime (N) and discount rate (i) are considered to be 20 years and 10%, respectively.

**5-  Validation**

In order to evaluate the accuracy of the model, the values of some important parameters calculated in this study are compared with those of the Ref. [18] that are shown in Table 3. The Root-Mean-Square deviation (RMSE) is used to calculate the error. The value of this parameter is calculated as 0.7, which indicates the validity of the present work.

**Table 3. Comparison of results calculated in this paper with those of the Ref. [18]**

| Parameter | Values calculated in this paper | Values presented in Ref. [7] |
|---|---|---|
| Vapor generator temperature, $T_g(K)$ | 395 | 395 |
| Condenser temperature, $T_c(K)$ | 298 | 298 |
| Evaporator temperature, $T_e(K)$ | 280 | 280 |
| System input power, $Q_g(kW)$ | 251.65 | 254.30 |
| Pump consumption power, $P_{pump}(kW)$ | 1.6 | 1.4 |
| Turbine production power, $P_{Tur}(kW)$ | 27.4 | 29.3 |
| Net production power, $P_{net}(kW)$ | 25.8 | 27.9 |
| Thermal efficiency, $\eta_{Thm}(\%)$ | 36.64 | 34.1 |
| Exergy efficiency, $\eta_{Exg}(\%)$ | 53.28 | 56.8 |

**6-  Results and discussion**

Table 4 shows the thermodynamic characteristics including temperature, pressure, mass flow rate, enthalpy and entropy for different points of the combined system for R245fa working fluid. The operational parameters of the system are also shown in Table 5 for different working fluids. As shown in Table 5, the total input energies and exergies of the system are approximately the same for all the working fluids, and their values are 328.9 kW and 308.2 kW, respectively. The data from this table show that the highest daily thermal efficiency ($\eta_{Thm}$) and exergy efficiency ($\eta_{Exg}$) belongs to the R123 working fluid (38.61% and 17.03%, respectively) due to its higher output energy and exergy, while the lowest total cost rate ($\dot{Z}_{total}$) belongs to the R600a working fluid and its value is 10685 $/year. The cost rate of each component of the system for different working fluids is shown in Table 6. According to Table 6, for R245fa working fluid, the storage tank shows the highest cost rate value (21169.42 $/year) and heater shows the lowest cost rate value (318.01 $/year).

---

[2] Data are obtained from Apricus corporation

**Table 4. Thermodynamic properties for different points of the combined system for R245fa working fluid**

| Sta te | Fluid | $T(K)$ | $P(MPa$ | $\dot{m}(kg/s)$ | $h(kJ/kg)$ | $s(kJ/Kg.K)$ |
|---|---|---|---|---|---|---|
| 1 | R245fa | 298 | 0.149 | 1 | 232.3 | 1.113 |
| 2 | R245fa | 298.6 | 1.5 | 1 | 233.4 | 1.113 |
| 3 | R245fa | 383.9 | 1.5 | 1 | 482.7 | 1.806 |
| 4 | R245fa | 349 | 0.401 | 1 | 466.5 | 1.83 |
| 5 | R245fa | 331.5 | 0.401 | 1 | 448.1 | 1.776 |
| 6 | R245fa | 323.2 | 0.149 | 1.331 | 446.6 | 1.828 |
| 7 | R245fa | 293.6 | 0.149 | 1.331 | 226.4 | 1.093 |
| 8 | R245fa | 280 | 0.149 | 0.331 | 208.8 | 1.031 |
| 9 | R245fa | 280 | 0.0717 | 0.331 | 208.8 | 1.032 |
| 10 | R245fa | 280 | 0.0717 | 0.331 | 409.5 | 1.749 |
| 11 | Water | 293.2 | 0.3 | 2.647 | 59.02 | 0.2096 |
| 12 | Water | 287.2 | 0.3 | 2.647 | 84.12 | 0.2961 |
| 13 | Water | 293.2 | 0.3 | 14.01 | 84.12 | 0.2961 |
| 14 | Water | 298.2 | 0.3 | 14.01 | 105 | 0.3669 |
| 15 | Water | 333.2 | 0.14 | 0.126 | 251.3 | 0.8311 |
| 16 | - | - | - | - | - | - |
| 17 | - | - | - | - | - | - |
| 18 | Water | 388.2 | 1.5 | 3.424 | 483.7 | 1.473 |
| 19 | Water | 390.5 | 1.5 | 3.424 | 493.4 | 1.498 |
| 21 | Water | 390.5 | 1.5 | 3.424 | 493.4 | 1.498 |
| 22 | Water | 397.9 | 1.5 | 3.424 | 525 | 1.578 |

**Table 5. Performance of the system for different working fluids**

| Parameter | R245fa | R123 | R600a | R134a |
|---|---|---|---|---|
| Input energy, $\dot{E}$ | 328.956 | 328.956 | 328.956 | 328.956 |
| Input exergy, $\dot{E}x$ (kW) | 308.2 | 308.2 | 308.2 | 308.2 |
| Daily thermal | 30.38 | 38.61 | 15.54 | 36.45 |
| Daily exergy efficiency, | 5.636 | 17.03 | 1.064 | 14.71 |
| Net power production, | 15.02 | 50.47 | 2.121 | 49.47 |
| Total cost rate, $\dot{Z}_{total}$ ($/year) | 13938 | 19333 | 11246 | 19141 |

**Table 6.** Cost rate of each component of the combined system for different working fluids

| Component | R245fa | R600a | R123 | R134a |
|---|---|---|---|---|
| Pump | 571.34 | 643.1 | 990.82 | 983.82 |
| Vapor generator | 2928 | 2006 | 3921 | 3914 |
| Turbine | 3187 | 3082.5 | 5800 | 5793 |
| Heater | 318.01 | 404.05 | 140.71 | 133.71 |
| Ejector | 2713 | 1806 | 4502 | 4495 |
| Condenser | 1945.8 | 3292.5 | 5984 | 5972 |
| Expansion valve and evaporator | 787.6 | 1600.1 | 878.8 | 866.8 |
| Thermal storage tank | 21169.42 | 21165.26 | 21162.54 | 21153.54 |
| Solar collector | 9039 | 9039 | 21162.54 | 9039 |

As already mentioned, the combination of water and CuO are also used in solar collector subsystem instead of pure water. The effect of volume fraction of CuO nanoparticles on operational parameters of the system, including thermal efficiency and exergy efficiency, has been investigated. The effect of increasing the volume fraction of CuO nanoparticles on thermal efficiency and exergy efficiency is shown in Fig. 2 and Fig. 3, respectively. Increasing the volumetric fraction of CuO nanoparticles up to 2% increases the heat transfer coefficient of the collector by 5.56%, in comparison with the water. By increasing this thermodynamic parameter ($\varphi_{np}$), the exergy efficiency of the combined system for the working fluids including R245fa, R600a, R123, and R134a increases by 4.4%, 4.85%, 4.6% and 2.91%, respectively.
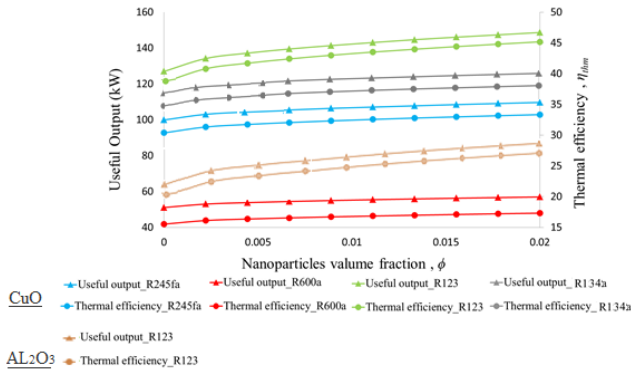
**Figure 2. The effect of increasing volumetric fraction of CuO nanoparticles on the thermal efficiency and total output power**
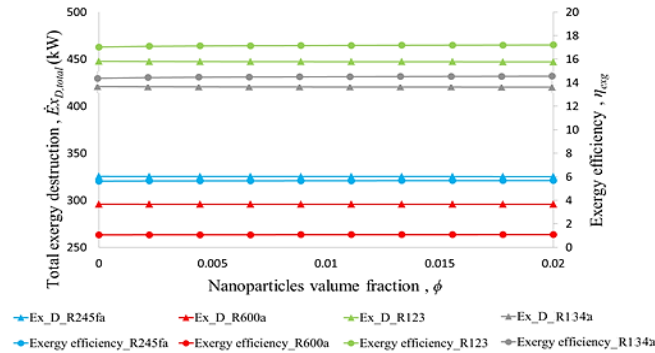


**Figure 3. The effect of increasing volumetric fraction of CuO nanoparticles on the exergy efficiency and total exergy destruction**

## 7- Optimization

In this section, the multi-objective optimization of the combined cycle is described. SPEA2, MOPSO, NSGA-II Algorithms are used to optimize the combined system and that code has been developed in MATLAB software. The summation of some important parameters including daily thermal efficiency, exergy efficiency, total heat exchangers area, and total cost rate of products are considered as the objective function and the affecting parameters of the system performance including solar collector area, solar collector tilt angle, volumetric fraction of CuO nanoparticles in water, pinch point temperature difference, and turbine inlet pressure are considered as decision variables in optimization algorithm. The feasible range of decision variables for different working fluids is shown in Table 7.

**Table 7. The feasible range of decision variables for different working fluids**

| decision variable | R245fa | R600a | R123 | R134a |
|---|---|---|---|---|
| Solar collector area ($m^2$) | 375-500 | 375-500 | 375-500 | 375-500 |
| Tilt angle (*degrees*) | 5-30 | 5-30 | 5-30 | 5-30 |
| Volumetric fraction (%) | 0-2 | 0-2 | 0-2 | 0-2 |
| Pinch point temperature difference (°C) | 5-10 | 5-10 | 5-10 | 5-10 |
| Turbine inlet pressure (*kPa*) | 1300-1630 | 650-1000 | 1330-1630 | 1300-1630 |

In this study, two scenarios are considered for multi-objective optimization of the system. The objective of the optimization in the first scenario is maximizing the thermal efficiency and exergy efficiency, and on the other hand, minimizing the total heat transfer area which can be written as follows:

$$Max(f_1(\varphi_{np}, P_{gen}, \Delta T_{Pinch}, \beta_{Sc}, A_{FPC}) =$$
$$w_1\eta_{thm} + w_2\eta_{exg} + w_3(1 - A_{total})) \qquad (17)$$

Where $w_1$ is the weight of the thermal efficiency, $w_2$ is the weight of the exergy efficiency, and $w_3$ is the weight of the total heat exchanger area in the objective function. Constraints on the weights are written as follows:

$$0 \leq w_1, w_2, w_3 \leq 1 \qquad (18)$$
$$w_1 + w_2 + w_3 = 1 \qquad (19)$$

The objective of the optimization in the second scenario is simultaneously maximizing the thermal efficiency and exergy efficiency, and on the other hand, minimizing the total cost rate of products which can be written as follows:

$$Max(f_2(\varphi_{np}, P_{gen}, \Delta T_{Pinch}, \beta_{Sc}, A_{FPC}) =$$
$$w_4\eta_{thm} + w_5\eta_{exg} + w_6(1 - \dot{C}_{total,P})) \qquad (20)$$

Where $w_4$ is the weight of the thermal efficiency, $w_5$ is the weight of the exergy efficiency, and $w_6$ is the weight of the total cost rate of products in the objective function. Constraints on the weights are written as follows:

$$0 \leq w_4, w_5, w_6 \leq 1 \qquad (21)$$
$$w_4 + w_5 + w_6 = 1 \qquad (22)$$

For each given weighting coefficients, different values are obtained for the objective function. In this study, 40 different weight coefficients are selected to evaluate the objective function. The weight coefficients corresponding to the greatest objective function value are the desired values. Table 8 shows the results obtained for the variables and objective functions for the first scenario and for different working fluids in comparison with the base case. Similarly, Table 9 shows the results obtained for the variables and objective functions for the second scenario and for different working fluids in comparison with the base case. For the first scenario, according to Table 8, R123 has the highest daily thermal efficiency and exergy efficiency with the values of 53.45% and 22.64%, respectively, while R600a has the lowest total heat exchanger with the value of 23.05 $m^2$. Similarly, for the second scenario, as shown in Table 9, R123 working fluid has the highest daily thermal efficiency and exergy efficiency compared to the R245fa, R600a, and R134a with the values of 52.57% and 22.23%, respectively. R600a shows the lowest total cost rate of products with the value of 9856 $/year.

## 8-Conclusion

A novel combined cooling, heating, and power system driven by solar energy and geothermal energy based on organic Rankine cycle was investigated in the present study. The performance of the combined system was evaluated using two important indices including daily thermal efficiency and daily exergy efficiency. The high thermal and exergy efficiencies are not only purposes of a system design. For instance, the lower total heat exchanger area and total cost rate of products can be considered as important advantages of a CCHP system. For this reason, the summation of four mentioned parameters including daily thermal efficiency, daily exergy efficiency, total heat exchanger area, and total cost rate of products are considered as the objective function of the system optimization in two scenarios. The main results obtained from this study can be summarized as follows:

**First scenario:**

I. Implementation of the optimization algorithm improves daily thermal efficiency by SPEA2(11.02%, 18.53%, 35.84%, 28.28% ) MOPSO(14.3%, 24.9%, 38.43%, 31.0%) NSGA-II(14.25%, 19.24%, 38.20%, 30.64%) for the R245fa, R600a, R123, and R134a working fluids, respectively.

II. R123 has the highest daily thermal efficiency and exergy efficiency with the values of 52.45% and

21.64%, respectively, while R600a has the lowest total heat exchanger with the value of 22.05 $m^2$.

**Second scenario:**

I. Implementation of the optimization algorithm improves daily thermal efficiency by SPEA2(1.9%, 14.73%, 30.97%, 28.66%) MOPSO(1.15%, 21.17%, 38.1%, 34.1%) NSGA-II(1.42%, 19.24%, 34.60%, 32.26%) for the R245fa, R600a, R123, and R134a working fluids, respectively.

II. R123 has the highest daily thermal efficiency and exergy efficiency with the values of 50.57% and 21.23%, respectively, while R600a has the lowest total heat exchanger with the value of 22.05 $m^2$.

**Table 8. The results obtained for the variables and objective functions for the first scenario using three Algorithms in comparison with the Base Case (BC)**

| Parameters | R245fa | | | | R600a | | | | R123 | | | | R134a | | | |
|---|---|---|---|---|---|---|---|---|---|---|---|---|---|---|---|---|
| | BC | MOPSO | SPEA2 | NSGA-II | BC | MOPSO | SPEA2 | NSGA-II | BC | MOPSO | SPEA2 | NSGA-II | BC | MOPSO | SPEA2 | NSGA-II |
| $\eta_{thm}$ (%) | 30.38 | 34.73 | 33.73 | 34.71 | 15.54 | 19.42 | 18.42 | 19.35 | 38.61 | 53.45 | 52.45 | 53.36 | 36.45 | 47.76 | 46.76 | 47.62 |
| $\eta_{exg}$ (%) | 5.636 | 5.75 | 5.65 | 5.82 | 1.064 | 1.91 | 1.81 | 1.85 | 17.03 | 22.64 | 21.64 | 22.51 | 14.71 | 19.12 | 18.12 | 18.89 |
| $A_{total}$ (m$^2$) | 56.34 | 48.83 | 49.83 | 48.96 | 24.3 | 23.05 | 22.05 | 22.86 | 85.39 | 88.93 | 87.93 | 88.86 | 82.39 | 76.62 | 75.62 | 76.43 |
| $\varphi_{np}$ (-) | 0.00 | 0.000463 | 0.000463 | 0.000463 | 0.00 | 0.01885 | 0.01885 | 0.01885 | 0.00 | 0.02 | 0.02 | 0.02 | 0.00 | 0.0193 | 0.0193 | 0.0193 |
| $P_3$ (kPa) | 1500 | 1311 | 1311 | 1310 | 1500 | 1504 | 1504 | 1504 | 700 | 650.2 | 650.2 | 650.2 | 2100 | 790 | 790 | 790 |
| $\Delta T_{pinch}$ (°C) | 6.6 | 9.969 | 9.969 | 9.967 | 6.6 | 5.02 | 5.02 | 5.02 | 6.6 | 5.002 | 5.002 | 5.001 | 6.6 | 5.12 | 5.12 | 5.12 |
| $\beta_{Sc}$ (°) | 13 | 17.94 | 17.94 | 17.90 | 13 | 29.92 | 29.92 | 29.87 | 13 | 28.98 | 28.98 | 28.97 | 13 | 29.56 | 29.56 | 29.54 |
| $A_{FPC}$ (m$^2$) | 395 | 499.4 | 499.4 | 498.8 | 395 | 379.8 | 379.8 | 379.6 | 395 | 375 | 375 | 374.6 | 395 | 387 | 387 | 387 |

**Table 9. The results obtained for the variables and objective functions for the second scenario using Three Algorithms in comparison with the Base Case (BC)**

| Parameters | R245fa | | | | R600a | | | | R123 | | | | R134a | | | |
|---|---|---|---|---|---|---|---|---|---|---|---|---|---|---|---|---|
| | BC | MOPSO | SPEA2 | NSGA-II | BC | MOPSO | SPEA2 | NSGA-II | BC | MOPSO | SPEA2 | NSGA-II | BC | MOPSO | SPEA2 | NSGA-II |
| $\eta_{thm}$ (%) | 30.38 | 30.73 | 30.96 | 30.81 | 15.54 | 18.83 | 17.83 | 18.53 | 38.61 | 52.57 | 50.57 | 51.97 | 36.45 | 48.9 | 46.9 | 48.21 |
| $\eta_{exg}$ (%) | 5.636 | 5.94 | 5.74 | 5.83 | 1.064 | 1.908 | 1.608 | 1.863 | 17.03 | 22.23 | 21.23 | 21.56 | 14.71 | 19.03 | 16.03 | 18.77 |
| $C_{P,total}$ ($/year) | 13331 | 12403 | 12373 | 12390 | 10685 | 9856 | 9926 | 9889 | 18683 | 17403 | 17653 | 17523 | 18285 | 15847 | 15937 | 15850 |
| $\varphi_{np}$ (-) | 0.00 | 0.00 | 0.00 | 0.00 | 0.00 | 0.00231 | 0.00231 | 0.00231 | 0.00 | 0.01761 | 0.01761 | 0.01761 | 0.00 | 0.018 | 0.018 | 0.018 |
| $P_3$ (kPa) | 1500 | 1488 | 1488 | 1489 | 1500 | 1330 | 1330 | 1331 | 700 | 655.3 | 655.3 | 655.5 | 2100 | 780 | 780 | 781 |
| $\Delta T_{pinch}$ (°C) | 6.6 | 9.868 | 9.868 | 9.867 | 6.6 | 8.89 | 8.89 | 8.90 | 6.6 | 5.124 | 5.124 | 5.120 | 6.6 | 5.01 | 5.01 | 5.01 |
| $\beta_{Sc}$ (°) | 13 | 15.25 | 15.25 | 15.25 | 13 | 12.934 | 12.934 | 12.935 | 13 | 29.75 | 29.75 | 29.81 | 13 | 29.91 | 29.91 | 29.90 |
| $A_{FPC}$ (m$^2$) | 395 | 375.9 | 375.9 | 375.7 | 395 | 389.4 | 389.4 | 389.6 | 395 | 377.3 | 377.3 | 377.4 | 395 | 382.7 | 382.7 | 382.8 |

**References**

[1]    El-Emam R.S., and Dincer I., "Exergy and exergoeconomic analyses and optimization of geothermal organic Rankine cycle", Applied Thermal Engineering 2013; 59:435-444.

[2]    Li M., and Wang J., "Thermo-economic analysis and comparison of a CO2 transcritical power cycle and an organic Rankine cycle", Geothermics 2014; 50:101–111.

[3]    Torres-Reyes E, Picon Nunez M, Cervantes de Gortari J. "Exergy analysis and optimization of a solar-assisted heat pump." Energy 1998; 23:337–344.

[4]    Badescu V. "First and second law analysis of a solar assisted heat pump based heating system." Energy Convers Manage 2004; 43:2539–2552.

[5]    Aydın Dikici, Abdullah Akbulut. "Performance characteristics and energy–exergy analysis of solar-assisted heat pump system." Building and Environment; 2008; 43:1961–1972.

[6]    T. Yousefi, F. Veysi, E. Shojaeizadeh, S. Zinadini, An experimental investigation on the effect of Al2O3–H2O nanofluid on the efficiency of flat-plate solar collectors, Renewable Energy 2012; 39(1):293–298.

[7]    Zheng, B. and Y. Weng, *A combined power and ejector refrigeration cycle for low temperature heat sources.* Solar Energy, 2010. 84(5): p. 784-791.

[8]    R. Petela, "Exergy of undiluted thermal radiation," sol, Energy, vol. 74, no. 6. pp. 469-488, jun. 2003.

[9]    C. Zamfirescu and I. Dincer, "how Much Exergy one can obtain from incident solar radiation?," j. appl. Phys., vol. 105, no. 4, p. 044911, Feb. 2009.

[10]   F. Mohammadkhani, N. Shokati, S. M. S. Mahmoudi, M. Yari, and M. A. Rosen, "Exergoeconomic assessment and parametric study of a Gas Turbine-Modular Helium Reactor combined with two Organic Rankine Cycles," *Energy*, vol. 65, pp. 533–543, Feb. 2014.

[11]   R. S. El-Emam and I. Dincer, "Exergy and exergoeconomic analyses and optimization of geothermal organic Rankine cycle," *Appl. Therm. Eng.*, vol. 59, no. 1–2, pp. 435–444, Sep. 2013.

[12]   S. Martínez-Lera, J. Ballester, and J. Martínez-Lera, "Analysis and sizing of thermal energy storage in combined heating, cooling and power plants for buildings," *Appl. Energy*, vol. 106, pp. 127–142, Jun. 2013.

[13]   A. Bejan, G. (George) Tsatsaronis, and M. J. Moran, *Thermal design and optimization.* Wiley, 1996.

[14]   F. A. Boyaghchi and P. Heidarnejad, "Thermoeconomic assessment and multi objective optimization of a solar micro CCHP based on Organic Rankine Cycle for domestic application," *Energy Convers. Manag.*, vol. 97, pp. 224–234, Jun. 2015.

[15]   Haeseldonckx D, D'haeseleer W. The environmental impact of decentralised generation in an overall system context. Renew Sustain Energy Rev 2008; 12:437–454.

[16]   Wang S, Ma Z. Supervisory and optimal control of building HVAC systems: a review. HVAC&R Res 2008; 14:3–32.

[17]   Yokoyama R, Matsumoto Y, Ito K. Optimal sizing of a gas turbine cogeneration plant in consideration of its operational strategy. J Eng Gas Turbines Power 1994; 116:32.

[18]   Henze GP, Biffar B, Kohn D, Becker MP. Optimal design and operation of a thermal storage system for a chilled water plant serving pharmaceutical buildings. Energy Build 2008; 40:1004–1019.

[19]   Li Y, Wang X, Li D, Ding Y. A trigeneration system based on compressed air and thermal energy storage. Appl Energy 2012; 99:316–323.

[20]   H. Kian, A. Sedaghat, Multi-Criteria Optimization of a solar cooling system assisted ground source Heat Pump system, Modares Mechanical Engineering 2016; 16(1):51-62 (in Persian).

[21]   H. Park, J. Lee, W. Kim, Y. Kim, Performance optimization of a hybrid ground source heat pump with the parallel configuration of a ground heat exchanger and a supplemental heat rejecter in the cooling mode, international Journal of refrigeneration 2012; 35(6):1537-1546.

[22]   M. Alavy, HV. Nguyen, WH. Leong, SB. Dworkin, A methodology and computerized approach for optimizing hybrid ground source heat pump system design. Renewable Energy 2013; 57:404-412.